Robotica (2018) volume 36, pp. 225–240. © Cambridge University Press 2017
doi:10.1017/S0263574717000315

Dynamic analysis of Hexarot: axis-symmetric parallel manipulator

Siamak Pedrammehr†, Behzad Danaei‡, Hamid Abdi†*, Mehdi Tale Masouleh‡ and Saeid Nahavandi†

†*Institute for Intelligent Systems Research and Innovation, Deakin University, Waurn Ponds Campus, Victoria 3217, Australia*
‡*Human and Robot Interaction Laboratory, School of Electrical and Computer Engineering, University of Tehran, Tehran, Iran*

(Accepted June 27, 2017. First published online: July 17, 2017)

SUMMARY
In this study, the kinematics and dynamics of a six-degree-of-freedom parallel manipulator, known as Hexarot, are evaluated. Hexarot is classified under axis-symmetric robotic mechanisms. The manipulator comprises a cylindrical base column and six actuated upper arms, which are connected to a platform through passive joints and six lower arms. The actuators of the mechanism are located inside a cylindrical-shaped base, which allows the mechanism to rotate infinitely about the axes of the latter column. In the context of kinematics, the inverse-kinematic problem is solved using positions, velocities, and accelerations of the actuated joints with respect to the position, orientation, and motion of the platform. Accordingly, the main objective of this study is to dynamically model the manipulator using the Newton–Euler approach. For validation, the obtained dynamic model of the Hexarot manipulator is simulated in MATLAB based on the formulations presented in this paper. The kinematic and dynamic models of the manipulator are simulated for a given motion scenario using MATLAB and ADAMS. The results of the mathematical model obtained using MATLAB are in good agreement with that using the ADAMS model, confirming the effectiveness of the proposed mathematical model.

KEYWORDS: Parallel manipulator, Axis-symmetric robots, Hexarot, Kinematics, Dynamics, Newton–Euler method.

Nomenclature

Throughout the paper, the vectors are given in the base frame $\{\mathbf{W}\}$ except those indicated with the upper prefix P. For instance, $\bar{\mathbf{I}}_p$ is in frame $\{\mathbf{W}\}$ and ${}^{\mathrm{P}}\bar{\mathbf{I}}_p$ is in frame $\{\mathbf{P}\}$.

$\{\mathbf{P}\}$	Moving platform frame
$\{\mathbf{W}\}$	Base frame
$\mathbf{a}_{\mathrm{i}}$	Position vector of the ith universal joint
a_{i}	Length of the ith upper arm
$\mathbf{a}_{ai}$	Acceleration vector of the mass centers of the ith upper arm
$\mathbf{a}_{li}$	Acceleration vector of the mass centers of the ith lower arm
$\mathbf{c}_{\mathrm{i}}$	Unit vector along the direction of the ith upper arm
$\mathbf{F}_{Ai}$	Force exerted from the ith actuated joint to the ith upper arm
$\mathbf{F}_{\mathrm{ext}}$	External force acting on the origin of the moving frame platform
$\mathbf{F}_{Si}$	Reaction force of the moving platform acting on the ith lower arm
$\mathbf{F}^{a}_{Si}$	Component of reaction force of the moving platform acting along the ith lower arm

* Corresponding author. E-mail: hamid.abdi@deakin.edu.au

https://doi.org/10.1017/S0263574717000315 Published online by Cambridge University Press

$\mathbf{F}_{Si}^{n}$	Component of reaction force of the moving platform acting perpendicular to the ith lower arm
$\mathbf{F}_{Ui}$	Force exerted from the ith universal joint to the ith lower arm
g	Acceleration due to gravity
$\bar{\mathbf{I}}_{ai}$	Inertia tensor of the ith upper arm
$\bar{\mathbf{I}}_{li}$	Inertia tensor of the ith lower arm
$\bar{\mathbf{I}}_{p}$	Inertia tensor of the moving platform
${}^{\mathrm{P}}\bar{\mathbf{I}}_{p}$	Inertia tensor of the moving platform in frame $\{\mathbf{P}\}$
$\bar{I}_{aaai}$	Mass moment of the inertia along the axial direction of the ith upper arm
$\bar{I}_{aali}$	Mass moment of the inertia along the axial direction of the ith lower arm
$\bar{I}_{nnai}$	Mass moment of the inertia along the normal direction of the ith upper arm
$\bar{I}_{nnli}$	Mass moment of the inertia along the normal direction of the ith lower arm
$\mathbf{J}$	Overall Jacobian matrix
$\mathbf{J}_{D}$	Direct Jacobian matrix
$\mathbf{J}_{I}$	Inverse Jacobian matrix
$\mathbf{l}_{\mathrm{i}}$	Length vector of the ith lower arm
l_{i}	Length of the ith lower arm
m_{a}	Mass of the upper arm
m_{p}	Mass of the moving platform
m_{l}	Mass of the lower arm
$\mathbf{M}_{Ai}$	Moment exerted from the ith actuated joint to the ith upper arm
$\mathbf{M}_{\mathrm{ext}}$	External moment acting on the origin of the moving frame $\{\mathbf{P}\}$
$\mathbf{M}_{Ui}$	Moment exerted from the ith universal joint to the ith lower arm
M_{Ui}	Magnitude of $\mathbf{M}_{Ui}$
$\mathbf{n_i}$	Unit vector of the ith lower arm
$\mathbf{O}$	Reference point on the center of the moving platform; position vector of the moving-platform center
$\dot{\mathbf{O}}$	Linear velocity of the moving platform
$\ddot{\mathbf{O}}$	Linear acceleration of the moving platform
$\ddot{\mathbf{O}}_{g}$	Acceleration of the mass center of the moving platform
$\mathbf{p}_{i}$	Position of the ith spherical joint
${}^{\mathrm{P}}\mathbf{p}_{i}$	Position of the ith spherical joint in frame $\{\mathbf{P}\}$
r_{ai}	Distance between the mass center of the ith upper arm and corresponding actuated joint
r_{li}	Distance between the mass center of the ith lower arm and its corresponding universal joint
$\bar{\mathbf{r}}$	Vector for the mass center of the moving platform
${}^{\mathrm{P}}\bar{\mathbf{r}}$	Vector for the mass center of the moving platform in frame $\{\mathbf{P}\}$
$\mathbf{R}$, $\mathbf{R}_{\mathrm{ZYZ}}$	Rotation matrix (3×3)
$\mathrm{R_i}$	ith rotational joints
$\mathrm{s_1}$	Length of sides of the triangular-moving platform
$\mathrm{s_2}$	Distance between the spherical joint and vertex of the triangular-moving platform
$\mathrm{S_i}$	ith spherical joint
$\mathbf{t}_{\mathrm{i}}$	Unit vector normal to the two axes of the ith universal joint
t	Time
$\mathrm{U_i}$	ith universal joint
$\mathbf{u}_{\mathrm{i}}$	Unit vector fixed to the joint axis on the ith upper arm
$\mathbf{v}_{\mathrm{i}}$	Unit vector normal to $\mathbf{u}_{\mathrm{i}}$ and $\mathbf{n}_{\mathrm{i}}$
$\hat{\mathbf{Z}}$	Unit vector in the Z direction of $\{\mathbf{W}\}$
$\boldsymbol{\alpha}$	Angular acceleration of the moving platform
$\boldsymbol{\alpha}_{li}$	Angular acceleration of the ith lower arm
ϕ_i	Angle between the ith upper arm and x-axis of the reference frame $\{\mathbf{W}\}$
$\dot{\varphi}_i$	Angular velocity of the ith upper arm
$\ddot{\phi}_i$	Angular acceleration of the ith upper arm
$\boldsymbol{\theta}$	Orientation vector of the moving platform center

https://doi.org/10.1017/S0263574717000315 Published online by Cambridge University Press

$\theta_1, \theta_2, \theta_3$	Euler angles with time derivatives of $\dot{\theta}_1$, $\dot{\theta}_2$, and $\dot{\theta}_3$ and $\ddot{\theta}_1$, $\ddot{\theta}_2$, and $\ddot{\theta}_3$
τ_i	Actuation torque
ω_{ui}	Magnitude of the angular velocity of the ith lower arm relative to the ith upper arm in $\mathbf{u}_i$ direction
ω_{vi}	Magnitude of the angular velocity of the ith lower arm relative to the ith upper arm in $\mathbf{v}_i$ direction
$\boldsymbol{\omega}$	Angular velocity of the moving platform
$\boldsymbol{\omega}_{li}$	Angular velocity of the ith lower arm

1. Introduction

A number of six-degree-of-freedom (DOF) parallel manipulators have been proposed after the various applications of the Gough–Stewart platform[1] in different industrial contexts, including manipulators with axis-symmetric parallel mechanisms such as Hexarots.[2–5] Axis-symmetric parallel manipulators are a type of parallel mechanism comprising a central base column and an arm mechanism capable of infinite rotation about the central column.[2] From a mechanical perspective, axis-symmetric parallel manipulators have coaxial motor actuators.[6] The configuration and properties of the manipulator will not change even if all the arms simultaneously rotate about the central column. The kinematic and the dynamic modeling of the parallel manipulators are more complicated than their serial mechanism because of the closed-chain structure and kinematic constraints. An accurate dynamic model is essential for understanding the behavior of these mechanisms and control purposes. To the best of our knowledge, no mathematical model exists that depicts the dynamics of Hexarot manipulators.

In the literature, different approaches have been proposed for the kinematic and dynamic modeling of parallel manipulators, including virtual-work approach,[7–10] Kane method,[11–13] momentum approach,[14,15] Hamilton method,[16] screw theory,[17] and recursive matrix method.[18] The Euler–Lagrange and Newton–Euler methods are among the popular methods for dynamic modeling, which have been extensively used to model different robotic systems, including the parallel mechanisms. In the Euler–Lagrange method, the kinematic constraints of the manipulators are considered through Lagrange multipliers, leading to a system of differential equations, which are often complicated.

The Euler–Lagrange and Newton–Euler methods have been employed to obtain inverse dynamics of several parallel mechanisms.[19–22] By extending the Euler–Lagrange method, Guo and Li[23] combined the Euler–Lagrange method with the Newton–Euler method to derive a closed-form dynamic equation for the Gough–Stewart parallel manipulators. When using the Newton–Euler method, Newton Laws and Euler equation of rigid bodies are applied to each component of the manipulator, and the closed-form dynamic equation can be obtained by solving the equations. Do and Yang[24] and Pedrammehr et al.[25] employed this method for the inverse dynamic analysis of different types of Gough–Stewart platform mechanisms. Dasgupta and Mruthyunjaya[26] followed a similar approach for the same mechanism but the frictional forces of the joint and mass moment of inertia of the pods were considered. Dasgupta and Mruthyunjaya[27] obtained dynamic equations for a general class of Gough–Stewart mechanisms using the Newton–Euler approach. Harib and Srinivasan[28] employed the Newton–Euler method to study the effects of joint configuration on the angular velocities and accelerations of the pods. Mahmoodi et al.[29] used the Newton–Euler method to evaluate the inverse dynamics of a six-DOF flight simulator. They utilized body-coordinate frames for the platform and pods instead of inertial-coordinate frames. Furthermore, they considered the gyroscopic effects of the rotary parts within the pods to achieve a faster convergence rate. Pedrammehr et al.[30–34] and Afzali-Far et al.[35–37] improved the inverse dynamics of a hexapod table and presented the kinematic, dynamic, and vibrational analyses of this mechanism.

The following are the objectives of this study: developing a novel dynamic model for the Hexarot parallel manipulator and presenting the equations of motion for this mechanism, and validation of the proposed model via a simulation study using MATLAB and ADAMS.

The remainder of this paper is organized as follows: In Section 2, the Hexarot parallel manipulator is introduced. In Section 3, the kinematic model of the Hexarot is presented. In Section 4, the dynamic model of the Hexarot parallel manipulator is presented, which is the main contribution of this study. Section 5 demonstrates the simulation study conducted to validate the proposed dynamic model. Finally, the concluding remarks are given in Section 6.

https://doi.org/10.1017/S0263574717000315 Published online by Cambridge University Press

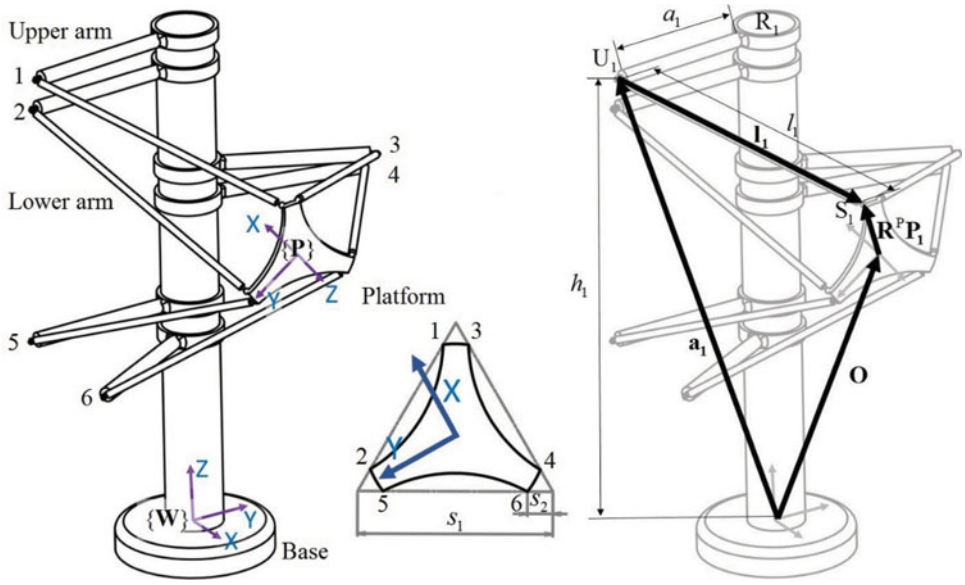


Fig. 1. Hexarot parallel mechanisms and representation of vectors for kinematics of first arm.

2. Hexarot Manipulators

The Hexarot parallel mechanism comprises a triangular-moving platform, a cylindrical central base column, and six actuated arms with coinciding axes of rotation, as shown in Fig. 1. The axis symmetric property of these manipulators refers to the common axis of rotation for the actuated joints. The platform of the Hexarot parallel robot is a rigid body capable of exhibiting six-DOF motions, including translation and rotation. Therefore, to fully describe the platform motion, six coordinate variables are required, where three variables can represent the position of a reference point located on the moving platform. The other three variables are used to describe the orientation of the moving platform.

To model the manipulator, a base frame $\{\mathbf{W}\}$ is assumed, which is located at the base of the manipulator. Moreover, the frame $\{\mathbf{P}\}$ is attached to the moving platform at the reference point $\mathbf{O}$. The position $\{\mathbf{P}\}$ with reference to frame $\{\mathbf{W}\}$ is $\mathbf{O} = [x\ y\ z]^{\mathrm{T}}$ and its orientation is obtained based on the Z–Y–Z Euler convention angles θ_1, θ_2 , and θ_3.

The Hexarot mechanism comprises six arms, wherein each arm comprises two links: upper arm a_i, and a lower arm l_i. As shown in Fig. 1, the ith upper arm is connected to the base column via the actuated rotational joint R_i and to the lower arm through the universal joint U_i. The other end of the lower arm is connected to the moving platform at point S_i through a spherical joint. Therefore, the moving platform comprises three pairs of spherical joints forming a triangular shape, which is shown in the center of Fig. 1. Six motors are located at the base column of the manipulator, helping the upper arms to rotate. The physical specifications of the Hexarot parallel manipulator are given in Appendix A. These specifications are used in Section 5 to develop the simulation models in MATLAB and ADMAS.

Having the actuators located in the central column helps reduce the weight of the moving parts, thereby resulting in motions with high velocity and acceleration. Furthermore, the Hexarot parallel robot has identical drivelines and identical upper and lower arms, thereby reducing the manufacturing cost. The Hexarot parallel robot is ideal for operations inside cylindrical spaces such as inside pipes, positioning or assembling tasks inside the body of an airplane. The robot is also used as a low mass and fast haptic device.[2]

3. Inverse Kinematics

The inverse-kinematic modeling of the Hexarot parallel robot helps determine the joint positions of the upper arms and their time derivatives when the position and orientation and their time derivatives of the moving platform are given.

https://doi.org/10.1017/S0263574717000315 Published online by Cambridge University Press

The mapping between the platform-coordinate and world-coordinate frames is achieved through a 3×3 rotation matrix $\mathbf{R} = \mathbf{R}_{ZYZ}(\theta_1, \theta_2, \theta_3)$ using the Euler angles θ_1, θ_2, and θ_3 as follows:

$$\mathbf{R} = \begin{bmatrix} \cos\theta_1 \cos\theta_2 \cos\theta_3 - \sin\theta_1 \sin\theta_3 & -\cos\theta_1 \cos\theta_2 \sin\theta_3 - \sin\theta_1 \cos\theta_3 & \cos\theta_1 \sin\theta_2 \\ \sin\theta_1 \cos\theta_2 \cos\theta_3 + \cos\theta_1 \sin\theta_3 & -\sin\theta_1 \cos\theta_2 \sin\theta_3 + \cos\theta_1 \cos\theta_3 & \sin\theta_1 \sin\theta_2 \\ -\sin\theta_2 \cos\theta_3 & \sin\theta_2 \sin\theta_3 & \cos\theta_2 \end{bmatrix}. \quad (1)$$

The angular velocity and acceleration of the moving platform with reference to the frame $\{\mathbf{W}\}$, i.e. $\boldsymbol{\omega} = [\,\omega_X \;\; \omega_Y \;\; \omega_Z\,]^{\mathrm{T}}$ and $\boldsymbol{\alpha} = [\,\alpha_X \;\; \alpha_Y \;\; \alpha_Z\,]^{\mathrm{T}}$, are obtained from the derivatives of the Euler angles $\dot{\theta}_1$, $\dot{\theta}_2$, and $\dot{\theta}_3$ and $\ddot{\theta}_1$, $\ddot{\theta}_2$, $\ddot{\theta}_3$, as follows:

$$\boldsymbol{\omega} = \begin{bmatrix} 0 & -\sin\theta_1 & \cos\theta_1 \sin\theta_2 \\ 0 & \cos\theta_1 & \sin\theta_1 \sin\theta_2 \\ 1 & 0 & \cos\theta_2 \end{bmatrix} \begin{bmatrix} \dot{\theta}_1 \\ \dot{\theta}_2 \\ \dot{\theta}_3 \end{bmatrix}, \quad (2)$$

$$\boldsymbol{\alpha} = \begin{bmatrix} 0 & -\sin\theta_1 & \cos\theta_1 \sin\theta_2 \\ 0 & \cos\theta_1 & \sin\theta_1 \sin\theta_2 \\ 1 & 0 & \cos\theta_2 \end{bmatrix} \begin{bmatrix} \ddot{\theta}_1 \\ \ddot{\theta}_2 \\ \ddot{\theta}_3 \end{bmatrix} + \begin{bmatrix} 0 & -\dot{\theta}_1 \cos\theta_1 & -\dot{\theta}_1 \sin\theta_1 \sin\theta_2 + \dot{\theta}_2 \cos\theta_1 \cos\theta_2 \\ 0 & -\dot{\theta}_1 \sin\theta_1 & \dot{\theta}_1 \cos\theta_1 \sin\theta_2 + \dot{\theta}_2 \sin\theta_1 \cos\theta_2 \\ 0 & 0 & -\dot{\theta}_2 \sin\theta_2 \end{bmatrix} \begin{bmatrix} \dot{\theta}_1 \\ \dot{\theta}_2 \\ \dot{\theta}_3 \end{bmatrix}. \quad (3)$$

3.1. Inverse-position kinematics

The position vector of the ith universal joint $\mathbf{a}_i$ with reference to the frame $\{\mathbf{W}\}$ is obtained as follows:

$$a_i = \begin{bmatrix} a_i \cos\varphi_i & a_i \sin\varphi_i & h_i \end{bmatrix}^{\mathrm{T}}, \quad (4)$$

where φ_i is the angle between the ith upper arm and x-axis of the frame $\{\mathbf{W}\}$. This angle indicates the rotation of the ith upper arm.

By considering the moving platform as an equilateral triangle, if s_1 is the length of its sides and s_2 is the distance between the spherical joint and vertex of the triangle (see Fig. 1), the positions of the spherical joint ${}^{\mathrm{P}}\mathbf{p}_i$ in the coordinate frame $\{\mathbf{P}\}$ can be obtained as follows:

$$\begin{aligned} {}^{\mathrm{P}}\mathbf{p}_1 &= \begin{bmatrix} \frac{(s_1 - s_2)}{2} & \frac{(-s_1 + 3s_2)}{2\sqrt{3}} & 0 \end{bmatrix}^{\mathrm{T}}, {}^{\mathrm{P}}\mathbf{p}_2 = \begin{bmatrix} \frac{s_2}{2} & \frac{(2s_1 - 3s_2)}{2\sqrt{3}} & 0 \end{bmatrix}^{\mathrm{T}}, \\ {}^{\mathrm{P}}\mathbf{p}_3 &= \begin{bmatrix} \frac{(s_1 - 2s_2)}{2} & \frac{-s_1}{2\sqrt{3}} & 0 \end{bmatrix}^{\mathrm{T}}, {}^{\mathrm{P}}\mathbf{p}_4 = \begin{bmatrix} \frac{-(s_1 - 2s_2)}{2} & \frac{-s_1}{2\sqrt{3}} & 0 \end{bmatrix}^{\mathrm{T}}, \\ {}^{\mathrm{P}}\mathbf{p}_5 &= \begin{bmatrix} \frac{-s_2}{2} & \frac{(2s_1 - 3s_2)}{2\sqrt{3}} & 0 \end{bmatrix}^{\mathrm{T}}, {}^{\mathrm{P}}\mathbf{p}_6 = \begin{bmatrix} \frac{-(s_1 - s_2)}{2} & \frac{(-s_1 + 3s_2)}{2\sqrt{3}} & 0 \end{bmatrix}^{\mathrm{T}}. \end{aligned} \quad (5)$$

The position of the ith spherical joint $\mathbf{p}_i = [\,p_{iX} \;\; p_{iY} \;\; p_{iZ}\,]^{\mathrm{T}}$ in the base frame is obtained using a combination of the translation and rotation transformations as follows:

$$\mathbf{p}_i = \mathbf{O} + \mathbf{R}\,{}^{\mathrm{P}}\mathbf{p}_i. \quad (6)$$

After determining the positions of the spherical and universal joints, i.e. $\mathbf{p}_i$ and $\mathbf{a}_i$, the length vector of the lower arm $\mathbf{l}_i$ can be obtained as follows:

$$l_i = \|\mathbf{p}_i - \mathbf{a}_i\|. \quad (7)$$

By substituting Eqs. (4) and (6) into Eq. (7), the following equation is obtained:

$$d_{i1} + d_{i2} \sin\varphi_i + d_{i3} \cos\varphi_i = 0, \quad (8)$$

https://doi.org/10.1017/S0263574717000315 Published online by Cambridge University Press

where

$$\begin{aligned} d_{i1} = {} & x^2 + y^2 + (z - h_i)^2 - l_i^2 + a_i^2 + p_{iX}^2 + p_{iY}^2 + p_{iZ}^2 \\ & + 2(z - h_i)(-p_{iX}\sin\theta_2\cos\theta_3 + p_{iY}\sin\theta_2\sin\theta_3 + p_{iZ}\cos\theta_2) \\ & - 2x(p_{iX}\sin\theta_1\sin\theta_3 + p_{iY}\sin\theta_1\cos\theta_3 - p_{iZ}\cos\theta_1\sin\theta_2) \\ & + 2y(p_{iX}\cos\theta_1\sin\theta_3 + p_{iY}\cos\theta_1\cos\theta_3 + p_{iZ}\sin\theta_1\sin\theta_2) \\ & + 2x\,p_{iX}\cos\theta_1\cos\theta_2\cos\theta_3 - 2x\,p_{iY}\cos\theta_1\cos\theta_2\sin\theta_3 \\ & + 2y\,p_{iX}\sin\theta_1\cos\theta_2\cos\theta_3 - 2y\,p_{iY}\sin\theta_1\cos\theta_2\sin\theta_3, \end{aligned} \tag{9}$$

$$\begin{aligned} d_{i2} = {} & -2a_i(y + p_{iX}\cos\theta_1\sin\theta_3 + p_{iY}\cos\theta_1\cos\theta_3 + p_{iZ}\sin\theta_1\sin\theta_2 \\ & + p_{iX}\sin\theta_1\cos\theta_2\cos\theta_3 - p_{iY}\sin\theta_1\cos\theta_2\sin\theta_3), \end{aligned} \tag{10}$$

$$\begin{aligned} d_{i3} = {} & -2a_i(x - p_{iX}\sin\theta_1\sin\theta_3 - p_{iY}\sin\theta_1\cos\theta_3 + p_{iZ}\cos\theta_1\sin\theta_2 \\ & + p_{iX}\cos\theta_1\cos\theta_2\cos\theta_3 - p_{iY}\cos\theta_1\cos\theta_2\sin\theta_3). \end{aligned} \tag{11}$$

In the above equations, φ_i can be obtained by substituting Eqs. (9)–(11) into Eq. (8) as follows:

$$\begin{aligned} \varphi_i &= -2\,\mathrm{atan}\left(\left(d_{i2} + \sqrt{-d_{i1}^2 + d_{i2}^2 + d_{i3}^2}\right)/(d_{i1} - d_{i3})\right) \quad \text{for} \quad i = 1, 2, 5, 6, \\ \varphi_i &= -2\,\mathrm{atan}\left(\left(d_{i2} - \sqrt{-d_{i1}^2 + d_{i2}^2 + d_{i3}^2}\right)/(d_{i1} - d_{i3})\right) \quad \text{for} \quad i = 3, 4. \end{aligned} \tag{12}$$

3.2. Inverse-velocity kinematics

By substituting Eq. (6) into Eq. (7) and using the time derivative on both sides of the resulting expression, the following equation is obtained:

$$\boldsymbol{\omega}_{li} \times \mathbf{l}_i = \dot{\mathbf{O}} + \boldsymbol{\omega} \times \mathbf{R}^{\mathrm{P}}\mathbf{p}_i - \dot{\boldsymbol{\varphi}}_i \times \mathbf{a}_i, \tag{13}$$

where $\boldsymbol{\omega}_{li}$ is the angular velocity of the ith lower arm, $\dot{\mathbf{O}}$ and $\boldsymbol{\omega}$ are, respectively, the linear and angular velocities of the moving platform in the frame $\{\mathbf{W}\}$, and $\dot{\boldsymbol{\varphi}}_i$ is the angular velocity of the ith upper arm.

Considering $\mathbf{n}_i$ as the unit vector of the ith lower arm (i.e. $\mathbf{l}_i = \mathrm{l}_i\mathbf{n}_i$) and knowing that $\dot{\boldsymbol{\varphi}}_i$ is only in the Z direction, the inner product of the two sides of Eq. (13) with $\mathbf{n}_i$, can be written as follows:

$$\dot{\varphi}_i(\mathbf{a}_i \times \mathbf{n}_i) \cdot \hat{\mathbf{Z}} = \dot{\mathbf{O}} \cdot \mathbf{n}_i + \left(\mathbf{R}^{\mathrm{P}}\mathbf{p}_i \times \mathbf{n}_i\right) \cdot \boldsymbol{\omega}. \tag{14}$$

In the above equation, $\hat{\mathbf{Z}} = [\,0\ 0\ 1\,]^{\mathrm{T}}$ is the unit vector along the Z direction of $\{\mathbf{W}\}$.

The angular velocity of the ith upper arm can be obtained by dividing the two sides of Eq. (14) by $(\mathbf{a}_i \times \mathbf{n}_i) \cdot \hat{\mathbf{Z}}$. The following can be written using Eq. (14):

$$\mathbf{J}_I\dot{\boldsymbol{\varphi}} = \mathbf{J}_D \begin{bmatrix} \dot{\mathbf{O}} \\ \boldsymbol{\omega} \end{bmatrix}. \tag{15}$$

https://doi.org/10.1017/S0263574717000315 Published online by Cambridge University Press

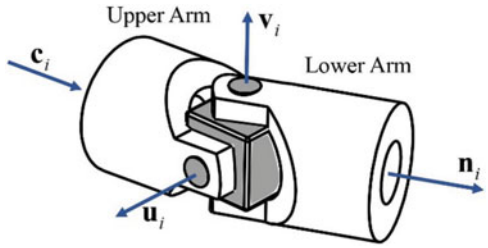


Fig. 2. 3D kinematic model of universal joint of Hexarot parallel robot.

In the above equation, $\mathbf{J}_I$ and $\mathbf{J}_D$ are, respectively, the inverse and direct Jacobian matrices, which can be obtained as follows:

$$\mathbf{J}_D = \begin{bmatrix} \mathbf{n}_1^{\mathrm{T}} & \left(\mathbf{R}^{\mathrm{P}}\mathbf{p}_1 \times \mathbf{n}_1\right)^{\mathrm{T}} \\ \vdots & \vdots \\ \mathbf{n}_6^{\mathrm{T}} & \left(\mathbf{R}^{\mathrm{P}}\mathbf{p}_6 \times \mathbf{n}_6\right)^{\mathrm{T}} \end{bmatrix}_{6\times 6} \text{ and } \mathbf{J}_I = \begin{bmatrix} (\mathbf{a}_1 \times \mathbf{n}_1)\cdot\hat{\mathbf{Z}} & \cdots & 0 \\ \vdots & \ddots & 0 \\ 0 & 0 & (\mathbf{a}_6 \times \mathbf{n}_6)\cdot\hat{\mathbf{Z}} \end{bmatrix}_{6\times 6}. \tag{16}$$

Hence, the overall Jacobian matrix $\mathbf{J}$ can be written as $\mathbf{J} = \mathbf{J}_I^{-1}\mathbf{J}_D$.

Figure 2 shows the universal joint of the Hexarot, where $\mathbf{c}_i$ and $\mathbf{n}_i$ are the unit vectors along the directions of the ith upper and lower arms, respectively. The unit vectors $\mathbf{u}_i$ and $\mathbf{v}_i$ indicate the kinematic model of the joint. The unit vector $\mathbf{u}_i$ is fixed along the joint axis of the upper arm, and $\mathbf{v}_i$ is orthogonal to $\mathbf{u}_i$ and $\mathbf{n}_i$. These vectors can be obtained as follows:

$$\mathbf{u}_i = \mathbf{c}_i \times \hat{\mathbf{Z}}, \tag{17}$$

$$\mathbf{v}_i = (1/\|\mathbf{u}_i \times \mathbf{n}_i\|)\,\mathbf{u}_i \times \mathbf{n}_i. \tag{18}$$

Based on the above definitions, the angular velocity of the ith lower arm $\boldsymbol{\omega}_{li}$ can be obtained as follows:

$$\boldsymbol{\omega}_{li} = \dot{\varphi}_i\hat{\mathbf{Z}} + \omega_{ui}\mathbf{u}_i + \omega_{vi}\,\mathbf{v}_i, \tag{19}$$

where ω_{ui} and ω_{vi} are, respectively, the magnitudes of the angular velocity in $\mathbf{u}_i$ and $\mathbf{v}_i$ directions relative to the ith upper arm.

By substituting Eq. (19) into Eq. (13) and using the inner product of $\mathbf{u}_i$ and $\mathbf{v}_i$, ω_{vi} and ω_{ui} can be obtained as follows:

$$\omega_{vi} = -1/\left((\mathbf{v}_i \times \mathbf{u}_i)\cdot\mathbf{l}_i\right)\left(\dot{\mathbf{O}}\cdot\mathbf{u}_i + \boldsymbol{\omega}\cdot\left(\mathbf{R}^{\mathrm{P}}\mathbf{p}_i \times \mathbf{u}_i\right) - \dot{\varphi}_i\hat{\mathbf{Z}}\cdot(\mathbf{p}_i \times \mathbf{u}_i)\right), \tag{20}$$

$$\omega_{ui} = 1/\left((\mathbf{v}_i \times \mathbf{u}_i)\cdot\mathbf{l}_i\right)\left(\dot{\mathbf{O}}\cdot\mathbf{v}_i + \boldsymbol{\omega}\cdot\left(\mathbf{R}^{\mathrm{P}}\mathbf{p}_i \times \mathbf{v}_i\right) - \dot{\varphi}_i\hat{\mathbf{Z}}\cdot(\mathbf{p}_i \times \mathbf{v}_i)\right). \tag{21}$$

3.3. Inverse-acceleration kinematics

The time derivative in Eq. (14) results in the angular acceleration of the ith upper arm $\ddot{\varphi}_i$ as follows:

$$\begin{aligned}\ddot{\varphi}_i = &\left(1/(\mathbf{a}_i \times \mathbf{n}_i)\cdot\hat{\mathbf{Z}}\right)\left(\ddot{\mathbf{O}}\cdot\mathbf{n}_i + \left(\mathbf{R}^{\mathrm{P}}\mathbf{p}_i \times \mathbf{n}_i\right)\cdot\boldsymbol{\alpha} + (\boldsymbol{\omega}_{li} \times \mathbf{n}_i)\cdot\dot{\mathbf{O}}\right.\\ &+ \left(\left(\boldsymbol{\omega} \times \mathbf{R}^{\mathrm{P}}\mathbf{p}_i\right) \times \mathbf{n}_i + \mathbf{R}^{\mathrm{P}}\mathbf{p}_i \times (\boldsymbol{\omega}_{li} \times \mathbf{n}_i)\right)\cdot\boldsymbol{\omega}\\ &\left. - \left(\left(\dot{\varphi}_i\hat{\mathbf{Z}} \times \mathbf{a}_i\right) \times \mathbf{n}_i + \mathbf{a}_i \times (\boldsymbol{\omega}_{li} \times \mathbf{n}_i)\right)\cdot\dot{\varphi}_i\hat{\mathbf{Z}}\right),\end{aligned} \tag{22}$$

where $\ddot{\mathbf{O}}$ and $\boldsymbol{\alpha}$ are the linear and angular accelerations of the moving platform, respectively.

https://doi.org/10.1017/S0263574717000315 Published online by Cambridge University Press

By differentiating Eq. (15) with respect to time, the angular acceleration of the upper arm can be rewritten in a closed and short mathematical form as follows:

$$\ddot{\boldsymbol{\varphi}} = \mathbf{J}\begin{bmatrix}\ddot{\mathbf{O}}\\ \boldsymbol{\alpha}\end{bmatrix} + \frac{\mathrm{d}\mathbf{J}}{\mathrm{d}t}\begin{bmatrix}\dot{\mathbf{O}}\\ \boldsymbol{\omega}\end{bmatrix}. \tag{23}$$

The time derivatives in Eqs. (13) and (19) result in the following equations for the angular acceleration of the ith lower arm denoted by $\boldsymbol{\alpha}_{li}$.

$$\boldsymbol{\alpha}_{li} \times \mathbf{l}_i + \boldsymbol{\omega}_{li} \times (\boldsymbol{\omega}_{li} \times \mathbf{l}_i) = \ddot{\mathbf{O}} + \boldsymbol{\alpha} \times \mathbf{R}^{\mathrm{P}}\mathbf{p}_i + \boldsymbol{\omega} \times \left(\boldsymbol{\omega} \times \mathbf{R}^{\mathrm{P}}\mathbf{p}_i\right) - \ddot{\varphi}_i\, \hat{\mathbf{Z}} \times \mathbf{a}_i - \dot{\varphi}_i \hat{\mathbf{Z}} \times \left(\dot{\varphi}_i\, \hat{\mathbf{Z}} \times \mathbf{a}_i\right), \tag{24}$$

$$\boldsymbol{\alpha}_{li} = \ddot{\varphi}_i \hat{\mathbf{Z}} + \alpha_{ui}\mathbf{u}_i + \alpha_{vi}\mathbf{v}_i + \omega_{ui}\left(\dot{\varphi}_i \hat{\mathbf{Z}} \times \mathbf{u}_i\right) + \omega_{vi}\left(\boldsymbol{\omega}_{li} \times \mathbf{v}_i\right), \tag{25}$$

where $\alpha_{ui} = d\omega_{ui}/dt$ and $\alpha_{vi} = d\omega_{vi}/dt$.

The accelerations are obtained by substituting Eq. (25) into Eq. (24) and using the inner product of the two sides of the resulting equation with $\mathbf{u}_i$ to solve for α_{vi} and with $\mathbf{v}_i$ to solve for α_{ui}.

$$\alpha_{vi} = (1/(\mathbf{u}_i \times \mathbf{v}_i)\cdot \mathbf{l}_i)\left(\ddot{\varphi}_i\, \mathbf{c}_i \cdot \mathbf{l}_i - \omega_{ui}\, \dot{\varphi}_i\, \hat{\mathbf{Z}} \cdot \mathbf{l}_i - \omega_{vi}\, (\mathbf{u}_i \times (\boldsymbol{\omega}_{li} \times \mathbf{v}_i)) \cdot \mathbf{l}_i + \left(\ddot{\mathbf{O}} + \boldsymbol{\alpha} \times \mathbf{R}^{\mathrm{P}}\mathbf{p}_i + \boldsymbol{\omega} \times \left(\boldsymbol{\omega} \times \mathbf{R}^{\mathrm{P}}\mathbf{p}_i\right) - \ddot{\varphi}_i\, \hat{\mathbf{Z}} \times \mathbf{a}_i - \dot{\varphi}_i\, \hat{\mathbf{Z}} \times \left(\dot{\varphi}_i\, \hat{\mathbf{Z}} \times \mathbf{a}_i\right) - \boldsymbol{\omega}_{li} \times (\boldsymbol{\omega}_{li} \times \mathbf{l}_i)\right) \cdot \mathbf{u}_i\right), \tag{26}$$

$$\alpha_{ui} = (1/(\mathbf{u}_i \times \mathbf{v}_i)\cdot \mathbf{l}_i)\left(\ddot{\varphi}_i \left(\hat{\mathbf{Z}} \times \mathbf{v}_i\right) \cdot \mathbf{l}_i - \omega_{ui}\, \left(\mathbf{v}_i \times \left(\dot{\varphi}_i\, \hat{\mathbf{Z}} \times \mathbf{u}_i\right)\right) \cdot \mathbf{l}_i - \omega_{vi}\, (\mathbf{v}_i \times (\boldsymbol{\omega}_{li} \times \mathbf{v}_i)) \cdot \mathbf{l}_i + \left(\ddot{\mathbf{O}} + \boldsymbol{\alpha} \times \mathbf{R}^{\mathrm{P}}\mathbf{p}_i + \boldsymbol{\omega} \times \left(\boldsymbol{\omega} \times \mathbf{R}^{\mathrm{P}}\mathbf{p}_i\right) - \ddot{\varphi}_i\, \hat{\mathbf{Z}} \times \mathbf{a}_i - \dot{\varphi}_i\, \hat{\mathbf{Z}} \times \left(\dot{\varphi}_i\, \hat{\mathbf{Z}} \times \mathbf{a}_i\right) - \boldsymbol{\omega}_{li} \times (\boldsymbol{\omega}_{li} \times \mathbf{l}_i)\right) \cdot \mathbf{v}_i\right). \tag{27}$$

In this section, the inverse kinematics of the Hexarot parallel manipulators is studied. In the next section, the mathematical model for the dynamics of this mechanism is developed.

4. Inverse Dynamics

In the mathematical model presented in this section, the gravity, inertia, Coriolis, centripetal, and external forces are considered. The friction and flexibility of the different elements of the mechanism are neglected because their effects are negligible. Further research is required to address these conditions. With this assumption, the first step in obtaining the dynamic model of the Hexarot parallel robot is to determine the acceleration vector of the mass centers of the upper and lower arms, i.e. $\mathbf{a}_{ai}$ and $\mathbf{a}_{li}$ as follows:

$$\mathbf{a}_{ai} = r_{ai}\ddot{\varphi}_i \left(\hat{\mathbf{Z}} \times \mathbf{c}_i\right) + r_{ai}\dot{\varphi}_i^2\, \hat{\mathbf{Z}} \times \left(\hat{\mathbf{Z}} \times \mathbf{c}_i\right), \tag{28}$$

$$\mathbf{a}_{li} = a_i\ddot{\varphi}_i\hat{\mathbf{Z}} \times \mathbf{c}_i + a_i\dot{\varphi}_i^2\hat{\mathbf{Z}} \times \left(\hat{\mathbf{Z}} \times \mathbf{c}_i\right) + r_{li}\left(\boldsymbol{\alpha}_{li} \times \mathbf{n}_i\right) + r_{li}\boldsymbol{\omega}_{li} \times \left(\boldsymbol{\omega}_{li} \times \mathbf{n}_i\right), \tag{29}$$

where r_{ai} is the distance between the mass center of the ith upper arm and corresponding actuated joint, and r_{li} is the distance between the mass center of the ith lower arm and its corresponding universal joint (see Fig. 3).

Figure 3 shows the forces and moments applied to the upper and lower arms. In this figure, $\mathbf{F}_{Ui}$ and $\mathbf{M}_{Ui}$ are the force and moment exerted by the ith universal joint to the ith lower arm, respectively. Similarly, $\mathbf{F}_{Ai}$ and $\mathbf{M}_{Ai}$ are the exerted force and moment by the ith actuated joint to the ith upper arm, respectively. $\mathbf{M}_{Ai}$ contains the actuation torque, which is referred to as τ_i.

The reaction force of the platform acting on the ith lower arm $\mathbf{F}_{Si}$ is assumed to have two components: a component along the ith lower arm $\mathbf{F}_{Si}^{a}$ and another component along the perpendicular

https://doi.org/10.1017/S0263574717000315 Published online by Cambridge University Press

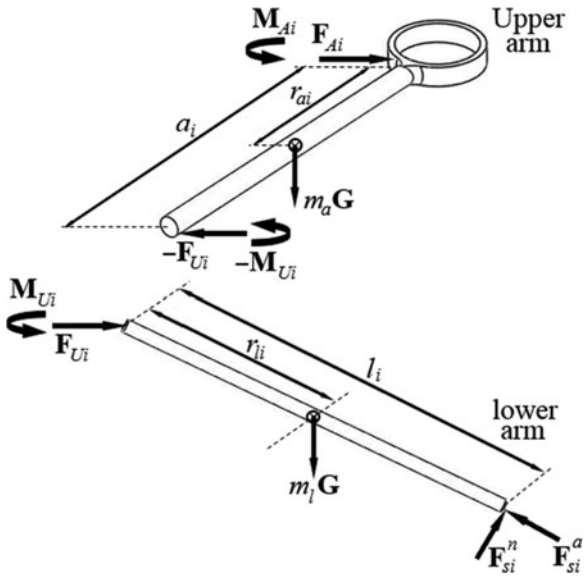


Fig. 3. Free body diagram of ith arm showing forces and moments for a pair of upper and lower arms.

direction to the direction of the ith lower arm $\mathbf{F}_{Si}^n$. Thus, $\mathbf{F}_{Si}$ can be written as follows:

$$\mathbf{F}_{Si} = \mathbf{F}_{Si}^a + \mathbf{F}_{Si}^n. \tag{30}$$

In the ith universal joint, by connecting the ith upper and lower arms, a moment component about an axis normal to the axes of the two revolute joints of the universal joint is transmitted to the corresponding lower arm. This reaction moment on the ith lower arm can be expressed as follows:

$$\mathbf{M}_{Ui} = M_{Ui}\mathbf{t}_i, \tag{31}$$

where M_{Ui} is the magnitude of $\mathbf{M}_{Ui}$, and $\mathbf{t}_i = \mathbf{v}_i \times \mathbf{u}_i$ is a unit vector normal to the two axes of the ith universal joint.

Referring to Fig. 3, the lower arm is subjected to a reaction force from the ith universal joint $\mathbf{F}_{Ui}$ and gravitational force $m_l\mathbf{G}$ with $\mathbf{G} = [\,0\ 0\ -g\,]^{\mathrm{T}}$, where g is the acceleration due to gravity.

Having established the external force and moment vectors on the ith lower arm and balancing the moment components about the ith universal joint, the following equation is obtained:

$$l_i\mathbf{n}_i \times \mathbf{F}_{Si}^n + \mathbf{M}_{Ui} + r_{li}\mathbf{n}_i \times m_l\mathbf{G} = \bar{\mathbf{I}}_{li}\boldsymbol{\alpha}_{li} + \boldsymbol{\omega}_{li} \times \bar{\mathbf{I}}_{li}\boldsymbol{\omega}_{li} + m_l r_{li}\mathbf{n}_i \times \mathbf{a}_{li}, \tag{32}$$

where $\bar{\mathbf{I}}_{li}$ is the inertia tensor of the ith lower arm in the base frame $\{\mathbf{W}\}$ with respect to the mass center of the lower arm.

Knowing the axis symmetric property of the six arms, computing the inertia tensor $\bar{\mathbf{I}}_{li}$ can be avoided by incorporating the scalar quantities $\bar{I}_{aali}$ and $\bar{I}_{nnli}$ representing the mass moments of the inertia along the axial and normal directions of the ith lower arm, respectively. Thus, the following equations are obtained:

$$\bar{\mathbf{I}}_{li}\boldsymbol{\alpha}_{li} = \bar{I}_{aali}\,(\mathbf{n}_i \cdot \boldsymbol{\alpha}_{li})\,\mathbf{n}_i + \bar{I}_{nnli}\mathbf{n}_i \times (\boldsymbol{\alpha}_{li} \times \mathbf{n}_i)\,, \tag{33}$$

$$\boldsymbol{\omega}_{li} \times \bar{\mathbf{I}}_{li}\boldsymbol{\omega}_{li} = \left(\bar{I}_{aali} - \bar{I}_{nnli}\right)(\mathbf{n}_i \cdot \boldsymbol{\omega}_{li})\,\boldsymbol{\omega}_{li} \times \mathbf{n}_i\,. \tag{34}$$

M_{Ui} is determined by the inner product of both sides of Eq. (32) with $\mathbf{n}_i$ and substituting Eqs. (31), (33), and (34) into the resulting equation, which leads to the following equation:

$$M_{Ui} = (1/\mathbf{t}_i \cdot \mathbf{n}_i)\,\bar{I}_{aali}(\mathbf{n}_i \cdot \boldsymbol{\alpha}_{li}). \tag{35}$$

https://doi.org/10.1017/S0263574717000315 Published online by Cambridge University Press

Considering that $\mathbf{n}_i$ is perpendicular to $\mathbf{F}^n_{Si}$, by substituting Eqs. (31), (33), and (34) into Eq. (32), the cross product $\mathbf{n}_i$ is used on both sides of the resulting equation to obtain the force $\mathbf{F}^n_{Si}$ as follows:

$$\begin{aligned}\mathbf{F}^n_{Si} = (1/l_i)\big(&-M_{Ui}\,\mathbf{t}_i \times \mathbf{n}_i - (r_{li}\mathbf{n}_i \times m_l\mathbf{G}) \times \mathbf{n}_i + \bar{I}_{nnli}\,(\boldsymbol{\alpha}_{li} \times \mathbf{n}_i)\\ &+ \left(\bar{I}_{aali} - \bar{I}_{nnli}\right)(\mathbf{n}_i \cdot \boldsymbol{\omega}_{li})\,(\boldsymbol{\omega}_{li} \times \mathbf{n}_i) \times \mathbf{n}_i + m_l r_{li}\,(\mathbf{n}_i \times \mathbf{a}_{li}) \times \mathbf{n}_i\big)\,. \end{aligned} \tag{36}$$

Having calculated the normal force component and reaction moment transmitted through the universal joint to the ith lower arm, i.e. $\mathbf{F}^n_{Si}$ and $\mathbf{M}_{Ui}$, the axial-force component can now be calculated, denoted by $\mathbf{F}^a_{Si}$. This force is along the axial direction of the corresponding lower arm; thus, $\mathbf{F}^a_{Si}$ can be expressed as follows:

$$\mathbf{F}^a_{Si} = F^a_{Si}\mathbf{n}_i, \tag{37}$$

where F^a_{Si} is the magnitude of $\mathbf{F}^a_{Si}$.

The six scalar quantities of F^a_{Si} for the six arms ($i = 1, 2..., 6$) can be determined from the force and moment equilibrium equations acting on the platform, which are as follows:

$$-\sum_{i=1}^{6} F^a_{Si}\mathbf{n}_i - \sum_{i=1}^{6} \mathbf{F}^n_{Si} + m_p\mathbf{G} + \mathbf{F}_{\text{ext}} = m_p\ddot{\mathbf{O}}_g, \tag{38}$$

where

$$\bar{\mathbf{I}}_p\boldsymbol{\alpha} + \boldsymbol{\omega} \times \bar{\mathbf{I}}_p\boldsymbol{\omega} + m_p\left(\bar{\mathbf{r}} \times \ddot{\mathbf{O}}_g\right) = m_p\bar{\mathbf{r}} \times \mathbf{G} - \sum_{i=1}^{6} F^a_{Si}\,\mathbf{R}\,{}^{\mathrm{P}}\mathbf{p}_i \times \mathbf{n}_i - \sum_{i=1}^{6} \mathbf{R}^{\mathrm{P}}\mathbf{p}_i \times \mathbf{F}^n_{Si} + \mathbf{M}_{\text{ext}}. \tag{39}$$

In the above equation, m_p and $\bar{\mathbf{I}}_p = \mathbf{R}^{\mathrm{P}}\bar{\mathbf{I}}_p\mathbf{R}^{\mathrm{T}}$ are the mass of the platform and its inertia tensor, respectively, which are calculated in the frame $\{\mathbf{W}\}$. ${}^{\mathrm{P}}\bar{\mathbf{I}}_p$ is the inertia tensor of the platform in the frame $\{\mathbf{P}\}$. $\mathbf{F}_{\text{ext}}$ and $\mathbf{M}_{\text{ext}}$ are the external force and moment acting at the origin of the moving frame $\{\mathbf{P}\}$, respectively, and $\ddot{\mathbf{O}}_g$ is the acceleration of the mass center of the moving platform, which is obtained as follows:

$$\ddot{\mathbf{O}}_g = \ddot{\mathbf{O}} + \boldsymbol{\alpha} \times \bar{\mathbf{r}} + \boldsymbol{\omega} \times (\boldsymbol{\omega} \times \bar{\mathbf{r}})\,, \tag{40}$$

where $\bar{\mathbf{r}} = \mathbf{R}\,{}^{\mathrm{P}}\bar{\mathbf{r}}$ denotes the vector for the mass center of the platform in the frame $\{\mathbf{W}\}$, and ${}^{\mathrm{P}}\bar{\mathbf{r}}$ is the same vector in the frame $\{\mathbf{P}\}$.

Finally, Eqs. (38) and (39) are combined to obtain the interacting forces between the lower arms and moving platform as follows:

$$\begin{bmatrix} F^a_{S1} \\ \vdots \\ F^a_{S6} \end{bmatrix} = \begin{bmatrix} \mathbf{n}_1 & \cdots & \mathbf{n}_6 \\ \mathbf{R}^{\mathrm{P}}\mathbf{p}_1 \times \mathbf{n}_1 & \cdots & \mathbf{R}^{\mathrm{P}}\mathbf{p}_6 \times \mathbf{n}_6 \end{bmatrix}^{-1} \mathbf{C}, \tag{41}$$

where

$$\mathbf{C} = \begin{bmatrix} -\sum_{i=1}^{6} \mathbf{F}^n_{Si} + m_p\mathbf{G} + \mathbf{F}_{\text{ext}} - m_p\ddot{\mathbf{O}}_g \\ m_p\bar{\mathbf{r}} \times \mathbf{G} - \sum_{i=1}^{6} \mathbf{R}^{\mathrm{P}}\mathbf{p}_i \times \mathbf{F}^n_{Si} + \mathbf{M}_{\text{ext}} - \bar{\mathbf{I}}_p\boldsymbol{\alpha} - \boldsymbol{\omega} \times \bar{\mathbf{I}}_p\boldsymbol{\omega} - m_p\left(\bar{\mathbf{r}} \times \ddot{\mathbf{O}}_g\right) \end{bmatrix}. \tag{42}$$

The other unknown forces and moments, shown in Fig. 3, can be obtained using Eq. (41). For this purpose, $\mathbf{F}_{Ui}$ can be determined by applying Newton's law to the ith lower arm as follows:

$$\mathbf{F}_{Ui} = m_l\,(\mathbf{a}_{li} - \mathbf{G}) - \mathbf{F}_{Si}. \tag{43}$$

https://doi.org/10.1017/S0263574717000315 Published online by Cambridge University Press

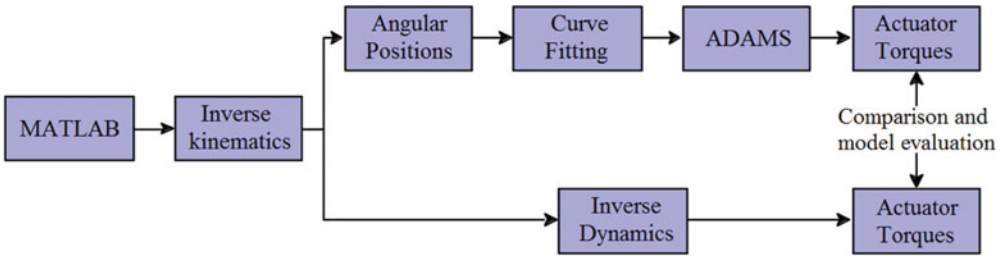


Fig. 4. Simulation process diagram.

Referring to Fig. 3, the force and moment exerted by the actuated joint to the ith upper arm are obtained using Newton's Law for the arm and moment balance equations about the actuated joint of this arm. Hence, $\mathbf{F}_{Ai}$ and $\mathbf{M}_{Ai}$ are given as follows:

$$\mathbf{M}_{Ai} = \mathbf{M}_{Ui} + a_i \mathbf{c}_i \times \mathbf{F}_{Ui} + m_a r_{ai} \mathbf{c}_i \times (\mathbf{a}_{ai} - \mathbf{G}) + \ddot{\varphi}_i \bar{\mathbf{I}}_{ai} \hat{\mathbf{Z}} + \dot{\varphi}_i^2 \hat{\mathbf{Z}} \times \left(\bar{\mathbf{I}}_{ai} \hat{\mathbf{Z}} \right), \tag{44}$$

$$\mathbf{F}_{Ai} = m_a (\mathbf{a}_{ai} - \mathbf{G}) + \mathbf{F}_{Ui}, \tag{45}$$

where $\bar{\mathbf{I}}_{ai}$ is the inertia tensor of the ith upper arm with respect to $\{\mathbf{W}\}$ at the mass center of the ith upper arm.

The mass inertia tensor of the ith upper arm is obtained using an approach similar to the one applied to the lower arm, i.e. Eqs. (33) and (34). Hence, the corresponding equations are obtained by using the scalar quantities $\bar{I}_{aaai}$ and $\bar{I}_{nnai}$ representing the mass moments of the inertia along the axial and the normal directions of the ith upper arm, respectively, as follows:

$$\ddot{\varphi}_i \bar{\mathbf{I}}_{ai} \hat{\mathbf{Z}} = \ddot{\varphi}_i \bar{I}_{aaai} \left(\mathbf{c}_i . \hat{\mathbf{Z}} \right) \mathbf{n}_i + \ddot{\varphi}_i \bar{I}_{nnai} \mathbf{c}_i \times \left(\hat{\mathbf{Z}} \times \mathbf{c}_i \right), \tag{46}$$

$$\dot{\varphi}_i^2 \hat{\mathbf{Z}} \times \left(\bar{\mathbf{I}}_{ai} \hat{\mathbf{Z}} \right) = \dot{\varphi}_i^2 \left(\bar{I}_{aaai} - \bar{I}_{nnai} \right) \left(\mathbf{c}_i \cdot \hat{\mathbf{Z}} \right) \hat{\mathbf{Z}} \times \mathbf{c}_i, \tag{47}$$

$\mathbf{M}_{Ai}$ represents the torques that are applied to the upper arm by the actuator of the arm and mechanical constraint of the based column. The actuation torque of the ith upper arm is $\tau_i = \mathbf{M}_{Ai} \cdot \hat{\mathbf{Z}}$, which is the required motor torque of the ith upper arm.

5. Simulation Study

To demonstrate the performance of the proposed mathematical dynamic model of the Hexarot parallel robot, a simulation study is performed. The physical parameters of the Hexarot parallel robot used in this simulation study are given in Appendix A. The results of this simulation are used to validate the proposed mathematical dynamic model of the Hexarot. Figure 4 shows the validation process, wherein the results of the mathematical model given in the previous section are compared with the corresponding results of the Hexarot model in ADMAS.

Hence, a MATLAB model is developed for the inverse kinematics and dynamics of the Hexarot, which is used to simulate a motion scenario of the manipulator. The motion scenario and initial conditions of the mechanism are given in Appendix B of this paper. An arbitrary path and speed could be specified for the motion scenario; however, the simulation path given in Appendix B is selected in such a way that it could also be simulated in ADAMS. The equation of motion for the actuator joints can be incorporated in ADAMS, which helps simulate the manipulator motion and required torque. This is performed by using the position profiles of the actuated joint obtained from the MATLAB model for the ADAMS model. To apply the position profile of the joint to the ADAMS model, first, a polynomial curve with six order is fitted to the joint-position profiles from the MATLAB, and the equation is used for ADAMS. The velocity and acceleration profiles of the joints, along with the joint-torque profiles, are obtained from the ADAMS model. In the last stage of the validation process, shown in Fig. 4, the results of the MATLAB and ADAMS models are compared and the differences between them are evaluated.

https://doi.org/10.1017/S0263574717000315 Published online by Cambridge University Press

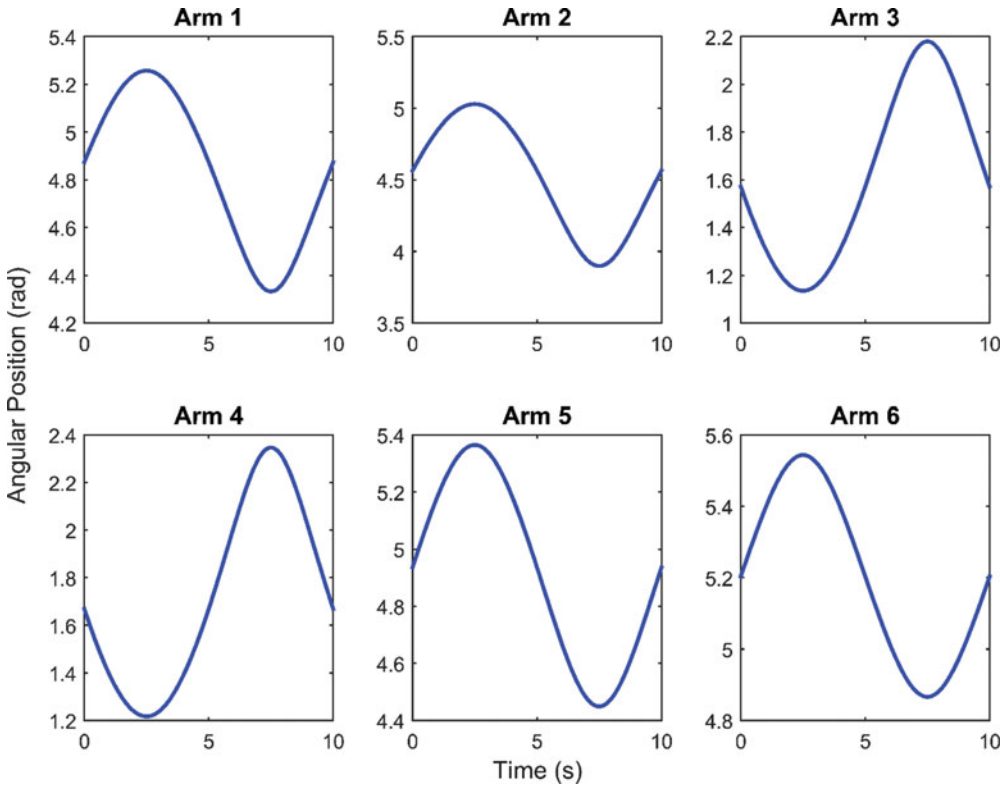


Fig. 5. Joint-position profiles of actuated arms for given motion scenario and path in Appendix B. This is obtained from the MATLAB model of the inverse kinematics of the Hexarot parallel robot.

In the simulation study, the motion scenario of the platform is a radial sinusoidal motion on a straight-line path along the x direction. The details of this motion scenario are given in Appendix B. The inverse kinematics, joint-angle positions, velocities, and accelerations of the arms, along with the joint-torque profiles of the mechanism are obtained from the MATLAB model. Similarly, the joint velocities, accelerations, and torque profiles are obtained from the ADAMS model. Figures 5-8 show the results of the MATLAB and ADAMS models. The most important result is shown in Fig. 8, where the actuation-torque profiles of the joints are obtained from the MATLAB and ADAMS models. This figure shows that the actuation-torque profiles of the MATLAB model are in good agreement with the corresponding torque obtained from the ADAMS model, thereby confirming the correctness of the mathematical model.

To quantify the similarity of the MATLAB and ADAMS models, the mean square error (MSE) between the outputs of the two models was determined. Figures 6–8 show the results. Some difference between the results of the MATLAB and ADAMS models exist, which can be justified as follows:

- The dimensions of the joints, or thickness of the parts, are not considered in the MATLAB model; therefore, small differences between the ADMAS and mathematical models exist.
- The curve-fitting process was performed only for the joint-angle positions. The error is nearly zero for the joint-angle positions; however, some error exists in the velocity and accelerations profiles. These errors are another source of the observed differences between the torque curves, shown in Fig. 8. It is observed that the difference between the torque profiles of the two models increases when the error in the acceleration and velocity increase.

6. Conclusions

This study investigated the kinematic and dynamic mathematical modeling of the Hexarot parallel manipulators. A novel dynamic model for the Hexarot manipulator was developed using the Newton–Euler approach. Based on the proposed mathematical model, a MATLAB model was developed. The

https://doi.org/10.1017/S0263574717000315 Published online by Cambridge University Press

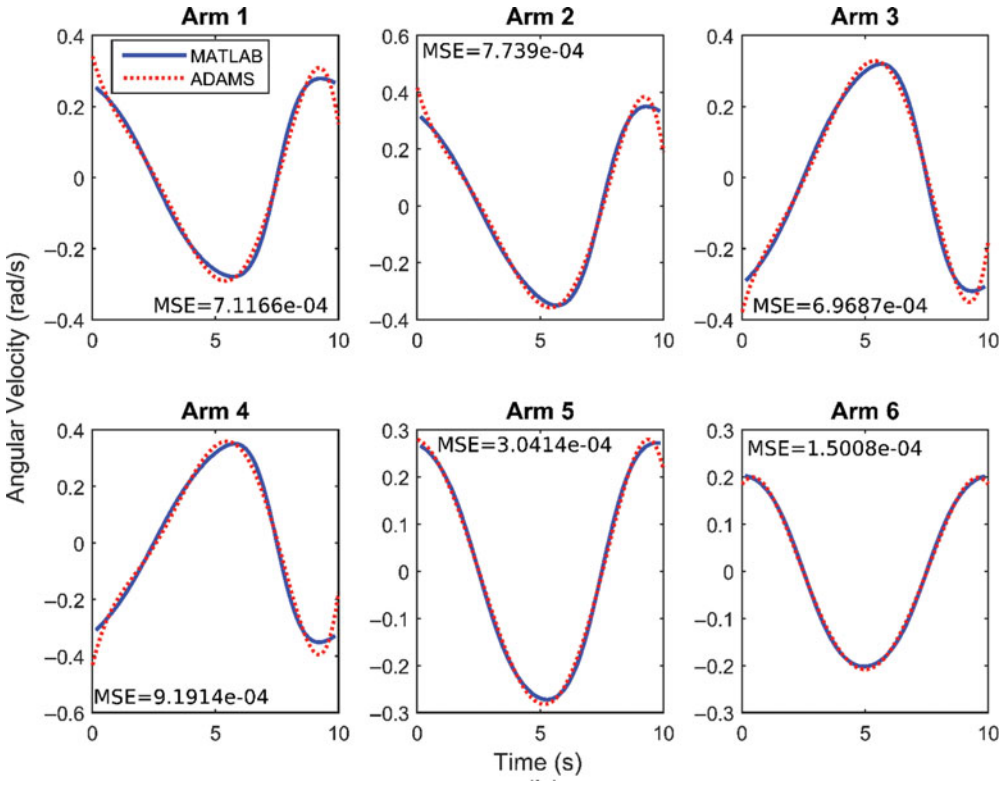


Fig. 6. Angular-velocity profiles obtained from MATLAB and ADAMS models. The dotted curve indicates the profiles obtained from ADAMS model.

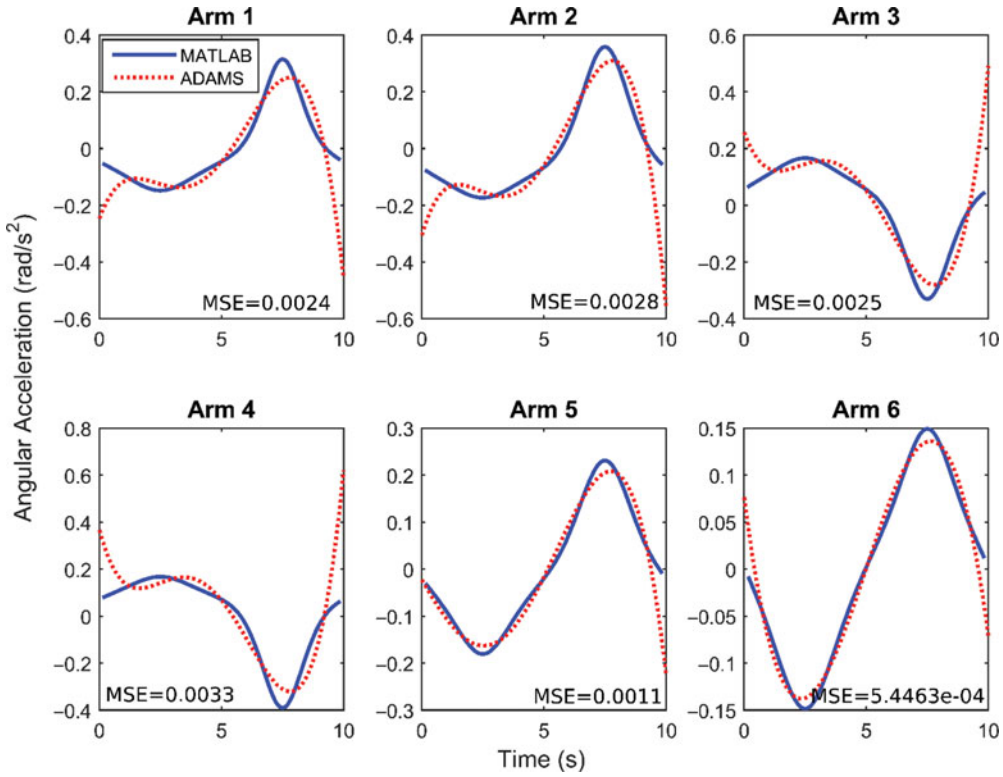


Fig. 7. Angular-acceleration profiles obtained from the MATLAB and ADAMS models. The dotted curve indicates the profiles obtained from ADAMS model.

https://doi.org/10.1017/S0263574717000315 Published online by Cambridge University Press

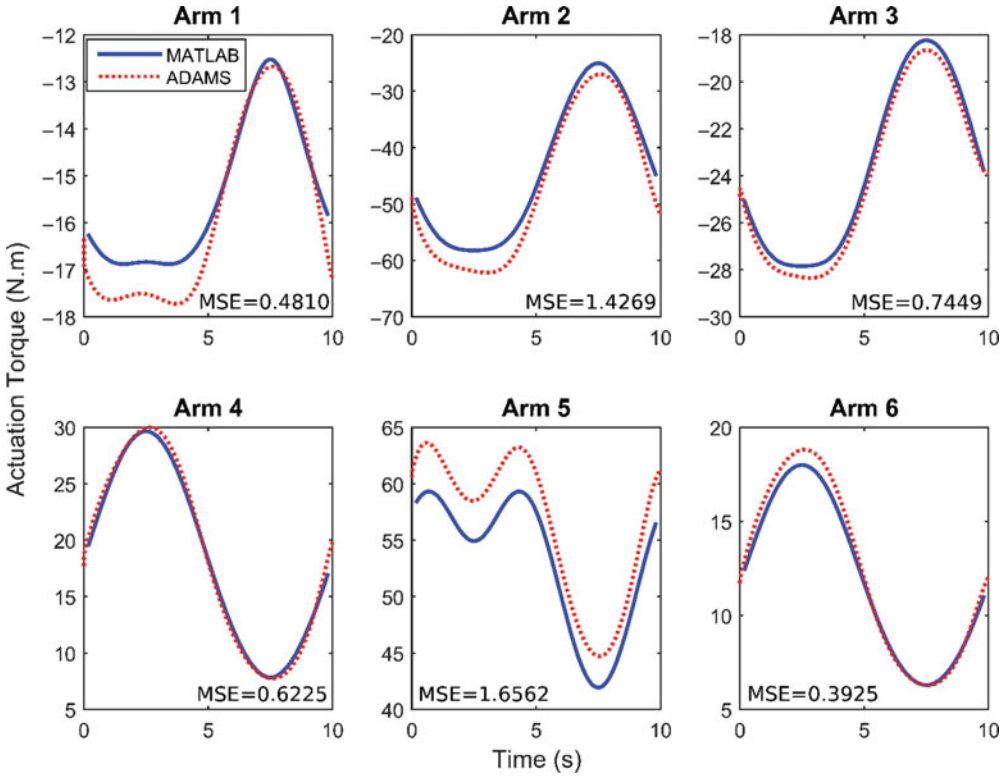


Fig. 8. Torque profiles obtained from the MATLAB and ADAMS models. The dotted curve indicates the profiles obtained from ADAMS model.

mathematical model was validated by comparing the results of the simulation study conducted using the MATLAB model with those of the ADAMS model. The results show that the proposed dynamic model appropriately represents the dynamic behavior of the Hexarot manipulator. Ongoing studies include dynamic identification and base-inertial-parameter determination of this manipulator.

References

1. D. Stewart, "A platform with six degrees of freedom," *Proc. Inst. Mech. Eng.* **180**, 371–386 (1965).
2. M. Isaksson, T. Brogårdh, M. Watson, S. Nahavandi, and P. Crothers, "The octahedral Hexarot—a novel 6-DOF parallel manipulator," *Mech. Mach. Theory* **55**, 91–102 (2012).
3. M. Isaksson, T. Brogårdh and S. Nahavandi, "Parallel manipulators with a rotation-symmetric arm system," *J. Mech. Des.* **134**, 114503 (2012).
4. M. R. C. Qazani et al., "Kinematic analysis and workspace determination of hexarot-a novel 6-DOF parallel manipulator with a rotation-symmetric arm system," *Robotica* **33**, 1686–1703 (2015).
5. M. R. C. Qazani, S. Pedrammehr, A. Rahmani, M. Shahryari, A. K. S. Rajab and M. M. Ettefagh, "An experimental study on motion error of hexarot parallel manipulator," *Int. J. Adv. Manuf. Technol.* **72**, 1361–1376 (2014).
6. M. Isaksson and M. Watson, "Workspace analysis of a novel six-degrees-of-freedom parallel manipulator with coaxial actuated arms," *J. Mech. Des.* **135**, 104501 (2013).
7. L.-W. Tsai, "Solving the inverse dynamics of a Stewart-Gough manipulator by the principle of virtual work," *J. Mech. Des.* **122**, 3–9 (2000).
8. S. Staicu, X.-J. Liu and J. Wang, "Inverse dynamics of the HALF parallel manipulator with revolute actuators," *Nonlinear Dyn.* **50**, 1–12 (2007).
9. Y. Zhao and F. Gao, "Inverse dynamics of the 6-dof out-parallel manipulator by means of the principle of virtual work," *Robotica* **27**, 259–268 (2009).
10. M. H. Abedinnasab and G. Vossoughi, "Analysis of a 6-DOF redundantly actuated 4-legged parallel mechanism," *Nonlinear Dyn.* **58**, 611–622 (2009).
11. M.-J. Liu, C.-X. Li and C.-N. Li, "Dynamics analysis of the Gough-Stewart platform manipulator," *IEEE Trans. Robot. Autom.* **16**, 94–98 (2000).
12. W. You, M.-X. Kong, Z.-J. Du and L.-N. Sun, "High efficient inverse dynamic calculation approach for a haptic device with pantograph parallel platform," *Multibody Syst. Dyn.* **21**, 233–247 (2009).

https://doi.org/10.1017/S0263574717000315 Published online by Cambridge University Press

13. P. Wu, H. Xiong and J. Kong, "Dynamic analysis of 6-SPS parallel mechanism," *Int. J. Mech. Mater. Des.* **8**, 121–128 (2012).
14. A. Mendes Lopes and F. Almeida, "The generalized momentum approach to the dynamic modeling of a 6-dof parallel manipulator," *Multibody Syst. Dyn.* **21**, 123–146 (2009).
15. A. M. Lopes, "Dynamic modeling of a Stewart platform using the generalized momentum approach," *Commun. Nonlinear Sci. Numer. Simul.* **14**, 3389–3401 (2009).
16. K. Miller, "Optimal design and modeling of spatial parallel manipulators," *Int. J. Robot. Res.* **23**, 127–140 (2004).
17. J. Gallardo, J. Rico, A. Frisoli, D. Checcacci and M. Bergamasco, "Dynamics of parallel manipulators by means of screw theory," *Mech. Mach. Theory* **38**, 1113–1131 (2003).
18. S. Staicu and D. Zhang, "A novel dynamic modelling approach for parallel mechanisms analysis," *Robot. Comput.-Integr. Manuf.* **24**, 167–172 (2008).
19. S. Pedrammehr, M. R. C. Qazani, H. Abdi and S. Nahavandi, "Mathematical modelling of linear motion error for Hexarot parallel manipulators," *Appl. Math. Modelling* **40**, 942–954 (2016).
20. G. Lebret, K. Liu and F. L. Lewis, "Dynamic analysis and control of a Stewart platform manipulator," *J. Robot. Syst.* **10**, 629–655 (1993).
21. Y. Ting, Y. S. Chen and H. C. Jar, "Modeling and control for a Gough-Stewart platform CNC machine," *J. Robot. Syst.* 21, 609–623 (2004).
22. A. Rahmani, A. Ghanbari and S. Pedrammehr, "Kinematic analysis for hybrid 2-(6-UPU) manipulator by wavelet neural network," *Adv. Mater. Res.* **1016**, 726–730 (2014).
23. H. Guo and H. Li, "Dynamic analysis and simulation of a six degree of freedom Stewart platform manipulator," *Proc. Inst. Mech. Eng. C: J. Mech. Eng. Sci.* **220**, 61–72 (2006).
24. W. Do and D. Yang, "Inverse dynamic analysis and simulation of a platform type of robot," *J. Robot. Syst.* **5**, 209–227 (1988).
25. S. Pedrammehr, M. Mahboubkhah and N. Khani, "Improved dynamic equations for the generally configured Stewart platform manipulator," *J. Mech. Sci. Technol.* **26**, 711–721 (2012).
26. B. Dasgupta and T. Mruthyunjaya, "A Newton-Euler formulation for the inverse dynamics of the Stewart platform manipulator," *Mech. Mach. Theory* **33**, 1135–1152 (1998).
27. B. Dasgupta and T. Mruthyunjaya, "Closed-form dynamic equations of the general Stewart platform through the Newton–Euler approach," *Mech. Mach. Theory* **33**, 993–1012 (1998).
28. K. Harib and K. Srinivasan, "Kinematic and dynamic analysis of Stewart platform-based machine tool structures," *Robotica* **21**, 541–554 (2003).
29. A. Mahmoodi, M. Menhaj and M. Sabzehparvar, "An efficient method for solution of inverse dynamics of Stewart platform," *Aircraft Eng. Aerospace Technol.* **81**, 398–406 (2009).
30. M. R. C. Qazani, S. Pedrammehr and M. J. Nategh, "A study on motion of machine tools' hexapod table on freeform surfaces with circular interpolation," *Int. J. Adv. Manuf. Technol.* **75**, 1763–1771 (2014).
31. S. Pedrammehr, M. Mahboubkhah and S. Pakzad, "An Improved Solution to the Inverse Dynamics of the General Stewart Platform," Proceedings of the Mechatronics (ICM), 2011 IEEE International Conference on, (2011) pp. 392–397.
32. S. Pedrammehr, H. Farrokhi, A. K. S. Rajab, S. Pakzad, M. Mahboubkhah, M. M. Ettefagh and M. H. Sadeghi, "Modal analysis of the milling machine structure through FEM and experimental test," *Adv. Mater. Res.* **383**, 6717–6721 (2012).
33. S. Pedrammehr, M. Mahboubkhah and N. Khani, "A study on vibration of Stewart platform-based machine tool table," *Int. J. Adv. Manuf. Technol.* **65**, 991–1007 (2013).
34. S. Pedrammehr, M. Mahboubkhah, M. R. C. Qazani, A. Rahmani and S. Pakzad, "Forced vibration analysis of milling machine's hexapod table under machining forces," *Strojniški Vestnik-J. Mech. Eng.* **60**, 158–171 (2014).
35. B. Afzali-Far, P. Lidström and K. Nilsson, "Parametric damped vibrations of Gough–Stewart platforms for symmetric configurations," *Mech. Mach. Theory* **80**, 52–69 (2014).
36. B. Afzali-Far and P. Lidström, "A Joint-Space Parametric Formulation for the Vibrations of Symmetric Gough-Stewart Platforms," **In**: (H. Selvaraj, D. Zydek, G. Chmaj eds.), Progress in Systems Engineering. Advances in Intelligent Systems and Computing, 366. Springer, Cham.
37. B. Afzali-Far, A. Andersson, K. Nilsson and P. Lidström, "Influence of strut inertia on the vibrations in initially symmetric Gough–Stewart Platforms—an analytical study," *J. Sound Vib.* **352**, 142–157 (2015).

Appendix A: Robot Specifications

The physical specifications of the Hexarot parallel manipulator are given in this appendix. The quantities are in SI units.

$$a_i = 0.63;\ l_i = 1 \text{ for } i = 1, 2..., 6.$$

$$s_1 = 0.46;\ s_2 = 0.06.$$

$$h_1 = 1.835; h_2 = 1.715;\ h_3 = 1.335.$$

$$h_4 = 1.215;\ h_5 = 0.835;\ h_6 = 0.715.$$

https://doi.org/10.1017/S0263574717000315 Published online by Cambridge University Press

The mass parameters of the platform and upper and lower arms are as follows:

$$m_{\mathrm{p}} = 5.76; m_{\mathrm{a}} = 7.628;\ m_1 = 2.43.$$

The distance between the mass center of each upper arm and related actuated joint is given as follows:

$$r_{\mathrm{a}i} = 0.248 \text{ for } i = 1, 2..., 6.$$

The distance between the mass center of each lower arm and related universal joint is given as follows:

$$r_{\mathrm{l}i} = 0.493 \text{ for } i = 1, 2..., 6.$$

The inertia tensor of the moving platform in frame $\{\mathbf{P}\}$ is given as follows:

$${}^{\mathrm{P}}\mathbf{I}_p = \begin{bmatrix} 0.0404 & 0 & 0 \\ 0 & 0.0404 & 0 \\ 0 & 0 & 0.0808 \end{bmatrix}.$$

The mass moments of inertia along the axial and normal directions of the ith upper arm at its mass center are given as follows:

$$\bar{I}_{aaai} = 1.68 \times 10^{-2};\ \bar{I}_{nnai} = 0.37 \text{ for } i = 1, 2 \ldots 6.$$

The mass moments of inertia along the axial and normal directions of the ith lower arm at its mass center are given as follows:

$$\bar{I}_{aali} = 1.88 \times 10^{-4};\ \bar{I}_{nnli} = 0.198 \text{ for } i = 1, 2 \ldots 6.$$

Appendix B: Simulation Specification

The position and orientation vectors of the moving platform center, i.e. $\mathbf{O} = [\, x \ y \ z \,]^{\mathrm{T}}$ and $\theta = [\, \theta_1 \ \theta_2 \ \theta_3 \,]^{\mathrm{T}}$, are expressed as functions of time t for each simulation path. The motion of the platform is a radial sinusoidal motion on a straight path along the x direction. In this case study, the platform moves away from the central column, and subsequently, returns back to its initial position.

$$\mathbf{F}_{\mathrm{ext}} = \begin{bmatrix} 0 & 0 & 0 \end{bmatrix}^{\mathrm{T}}; \mathbf{M}_{\mathrm{ext}} = \begin{bmatrix} 0 & 0 & 0 \end{bmatrix}^{\mathrm{T}},$$
$$\mathbf{O} = \begin{bmatrix} 0.8 + 0.3 \sin\left(\frac{2\pi t}{10}\right) & 0 & 1.5 \end{bmatrix}^{\mathrm{T}}; \theta = \begin{bmatrix} 0 & \pi/2 & \pi \end{bmatrix}^{\mathrm{T}}.$$

https://doi.org/10.1017/S0263574717000315 Published online by Cambridge University Press